

Systematic trends in YAlO_3 , SrTiO_3 , BaTiO_3 , BaZrO_3 (001) and (111) surface *ab initio* calculations

Roberts Eglitis*, J. Purans and A. I. Popov
*Institute of Solid State Physics, University of Latvia,
8 Kengaraga street, Riga LV1063, Latvia
rieglitis@gmail.com

Ran Jia
*Laboratory of Theoretical and Computational Chemistry,
Institute of Theoretical Chemistry, Jilin University,
Changchun 130023, P. R. China
jiaran@jl.u.edu.cn*

Received 5 September 2019
Revised 30 October 2019
Accepted 3 November 2019
Published 31 January 2020

The paper presents and discusses the results of performed calculations for YAlO_3 (111) surfaces using a hybrid B3LYP description of exchange and correlation. Calculation results for SrTiO_3 , BaTiO_3 and BaZrO_3 (111) as well as YAlO_3 , SrTiO_3 , BaTiO_3 and BaZrO_3 (001) surfaces are listed for comparison purposes in order to point out systematic trends common for these four ABO_3 perovskite (001) and (111) surfaces. According to performed *ab initio* calculations, the displacement of (001) and (111) surface metal atoms of YAlO_3 , SrTiO_3 , BaTiO_3 and BaZrO_3 perovskite, upper three surface layers for both AO and BO_2 (001) as well as AO_3 and B (111) surface terminations, in most cases, are considerably larger than that of oxygen atoms. The YAlO_3 , SrTiO_3 , BaTiO_3 and BaZrO_3 (001) surface energies for both calculated terminations, in most cases, are almost equal. In contrast, the (111) surface energies for both AO_3 and B-terminations are quite different. Calculated (111) surface energies always are much larger than the (001) surface energies. As follows from performed *ab initio* calculations for YAlO_3 , SrTiO_3 , BaTiO_3 and BaZrO_3 perovskites, the AO- and BO_2 -terminated (001) as well as AO_3 - and B-terminated (111) surface bandgaps are almost always reduced with respect to their bulk bandgap values.

Keywords: *Ab initio* calculation; YAlO_3 ; (111) surfaces; surface energies; B3LYP.

PACS numbers: 68.35.-p, 71.15.Mb, 71.20.-b, 73.20.At

1. Introduction

Surface and interface processes, happening in the ABO_3 perovskites and their complex nanostructures, as well as the original mechanisms of surface processes are

hot topics in modern physics nowadays.^{1–18} BaTiO₃, BaZrO₃, SrTiO₃ and YAlO₃ belong to the family of ABO₃ perovskite type oxides, and have a large number of technological applications besides being of large fundamental importance for basic research. The most important industrial applications of ABO₃ perovskites are charge storage devices, actuators, capacitors, fuel cells, water splitting applications, etc.^{19–22}

Thereby, it is self-evident that their neutral and consequently rather simple (001) surfaces, during the last quarter of the century, were intensively explored worldwide, both experimentally and theoretically.^{23–38} It is worth noting that the YAlO₃ (001) surface is different from most ABO₃ perovskite neutral (001) surfaces, since it consists of alternating charged YO and AlO₂ (001) planes.³⁹

From a theoretical point of view, it is considerably more easy to calculate the ABO₃ perovskite neutral (001) surfaces, than their complex, charged and polar (111) surfaces. This is the main reason why only a relatively small amount of theoretical and experimental papers exist dealing with ABO₃ perovskite polar, charged and thereby rather complex (111) surfaces.^{40–48}

The structure of SrTiO₃, BaTiO₃, BaZrO₃ and YAlO₃ crystals in their cubic phases represent an alternating sequence of layers consisting of two kinds of atoms. Namely, the ABO₃ perovskites in the [001] direction contain alternating and neutral AO and BO₂ planes, whereas in the [111] direction, they consist of alternating charged AO₃ and B planes. For example, at high-temperatures, BaTiO₃ perovskite has a cubic structure with the space group *Pm*3*m*, No. 221. As temperature lowers, BaTiO₃ undergoes three phase transitions from cubic to tetragonal and later to orthorhombic and rhombohedral phases. From another side, the BaZrO₃ crystal, as temperature lowers, always stays at its high symmetry cubic phase. At room-temperature, the SrTiO₃ crystal has a high symmetry cubic structure.

The aim of the work reported here was to perform the first *ab initio* calculations for complex, polar and charged YAlO₃ (111) surfaces and compare them with earlier calculation results for related ABO₃ perovskite (001) and (111) surfaces. After performing *ab initio* calculations for YAlO₃ (111) surfaces, the results for SrTiO₃, BaTiO₃, BaZrO₃ and YAlO₃ (001) and (111) surfaces were analysed as well as systematic trends common for all four mentioned ABO₃ perovskites were pointed out in a form easily readable for a broad audience of researchers.

2. Technical Calculation Details

2.1. YAlO₃ (111) surface atomic structure

The main problem in modeling the YAlO₃ polar and charged (111) surface is that, unlike the classical ABO₃ perovskite neutral (001) surfaces, it consists from charged planes YO₃ and Al, as shown in Fig. 1, assuming standard ionic charges of Y³⁺, Al³⁺ and O²⁻, the YAlO₃ (111) surfaces have been calculated using two-dimensional slabs, containing nine planes perpendicular to the [111] YAlO₃ crystal direction (Fig. 1). Namely, in order to calculate the YAlO₃ (111) surfaces, we

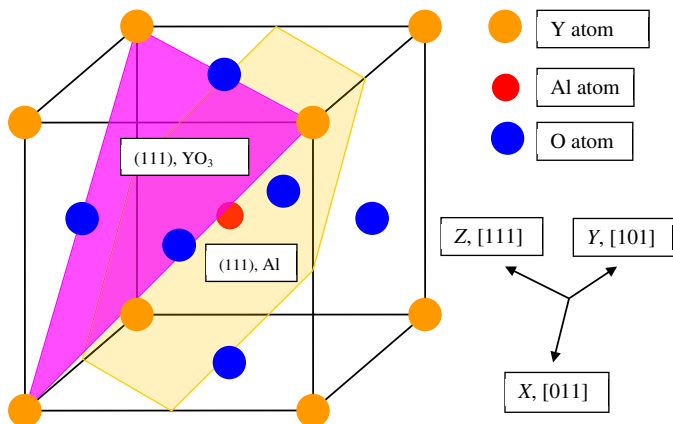


Fig. 1. (Color online) Sketch of the cubic $YAlO_3$ perovskite structure demonstrating two possible polar (111) surface terminations YO_3 and Al.

used symmetrical with respect to the mirror plane slabs consisting, in our case, from nine alternating Al and YO_3 layers. One of calculated nine layer slabs from both slab sides are terminated by Al planes and consists of a supercell containing 21 atoms ($Al-YO_3-Al-YO_3-Al-YO_3-Al-YO_3-Al$) [Fig. 2(a)]. The second calculated $YAlO_3$ (111) slab is terminated by YO_3 planes from both sides and consists of a supercell which contains 24 atoms ($YO_3-Al-YO_3-Al-YO_3-Al-YO_3-Al-YO_3$)

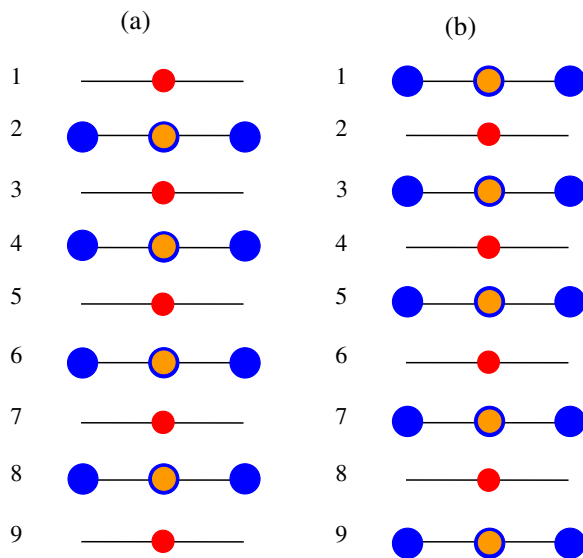


Fig. 2. (Color online) Side views of the slab geometries used by us to study the $YAlO_3$ polar (111) surfaces. (a) Nonstoichiometric Al-terminated nine layer $YAlO_3$ (111) slab and (b) nonstoichiometric YO_3 -terminated nine layer $YAlO_3$ (111) slab.

[Fig. 2(b)]. Thereby, both calculated slabs are nonstoichiometric and they have unit cell formulas $Y_4Al_5O_{12}$ and $Y_5Al_4O_{15}$, respectively (Fig. 2).

As it is known from early studies dealing with $SrTiO_3$, $BaTiO_3$, $CaTiO_3$ and $BaZrO_3$ polar and charged (111) surfaces,^{41,43,45,49,50} the strong electron redistribution are observed for such (111) terminations with aim to cancel the polarity, but the Al- and YO_3 -terminated $YAlO_3$ (111) surface maintain its insulating character, and such calculations are possible. Of course, it is impossible to carry out calculations for asymmetric slabs with different terminations, such as, for example, Al- YO_3 -Al- YO_3 -Al- YO_3 -Al- YO_3 . Such calculations will be impossible due to a large dipole moment for an asymmetric slab perpendicular to the z crystal direction.^{41,43,45}

2.2. Computational method and $YAlO_3$ (111) surface energy calculations

Ab initio calculations for $YAlO_3$ (111) surfaces have been performed by means of the CRYSTAL computer code.⁵¹ The most important feature of the CRYSTAL computer code for the study of the perovskite (001) and (111) surfaces is the isolated 2D slab model, which allows to perform surface calculations without artificial repetition along the z -axis. In order to perform calculations using the linear combination of atomic orbitals (LCAO) method and Gaussian-type functions (GTF) localized at atoms as the basis for an expansion of the crystalline orbitals, it is necessary to have optimized basis sets. For our $YAlO_3$ (111) surface calculations, we used exactly the same basis sets for Y, Al and O neutral atoms as in Ref. 39 for the $YAlO_3$ (001) surface atomic and electronic structure calculations. All $YAlO_3$ (111) surface calculations have been performed by means of B3LYP hybrid exchange-correlation functional including the hybrid of nonlocal Fock exact exchange, LDA exchange and Becke's gradient corrected exchange functional,⁵² in combination with the nonlocal gradient corrected correlation potential by Lee *et al.*⁵³ The reciprocal space integration was performed by sampling the Brillouin zone of the five atom $YAlO_3$ cubic unit cell with the $8 \times 8 \times 8$ and its (111) surfaces by $8 \times 8 \times 1$ times extended Pack-Monkhorst mesh.⁵⁴ It is worth to notice that we performed calculations by means of the B3LYP functional for $YAlO_3$ (111) and (001)³⁹ as well as for $SrTiO_3$,⁴⁵ $BaTiO_3$ ⁴¹ and $BaZrO_3$ ⁴³ (111) surfaces. For $SrTiO_3$,^{29,55,56} $BaTiO_3$ ^{5,55,56} and $BaZrO_3$ ^{34,55,56} (001) surfaces we performed calculations using the B3PW hybrid exchange-correlation functional.

Next, we calculated the $YAlO_3$ (111) surface and cleavage energies. It is clear that Al- and YO_3 -terminated $YAlO_3$ (111) surfaces are mutually complementary. Thereby, it is obvious that the cleavage energy is exactly the same for both YO_3 - and Al-terminated $YAlO_3$ (111) surfaces. Therefore, the cleavage energy for the complementary surface $E_{cl}(YO_3 + Al)$ can be derived from the total energies calculated for the unrelaxed slabs from the following equation:

$$E_{cl}(YO_3 + Al) = \frac{1}{4} [E_{slab}^{unrel}(Al) + E_{slab}^{unrel}(YO_3) - 9E_{bulk}], \quad (1)$$

where $E_{\text{slab}}^{\text{unrel}}$ (Al) is our calculated total energy of unrelaxed 21-atoms containing Al-terminated $YAlO_3$ (111) slab. $E_{\text{slab}}^{\text{unrel}}$ (YO_3) is the total energy for 24-atom YO_3 -terminated $YAlO_3$ (111) slab. E_{bulk} is the $YAlO_3$ total bulk energy per formula unit containing 5-atoms in the cubic structure. In Eq. (1) factor 9 before the E_{bulk} is due to the fact that 21-atom Al-terminated as well as 24-atom YO_3 -terminated $YAlO_3$ (111) slabs both together contain nine 5-atom $YAlO_3$ bulk unit cells. Factor $\frac{1}{4}$ in the right side of Eq. (1) means that totally four surfaces are created due the crystal cleavage. The relevant relaxation energies for each of the surfaces can be obtained by means of the following equation:

$$E_{\text{rel}}(\Psi) = \frac{1}{2} [E_{\text{slab}}^{\text{rel}}(\Psi) - E_{\text{slab}}^{\text{unrel}}(\Psi)], \quad (2)$$

where $\Psi = \text{Al}$ or YO_3 describes the $YAlO_3$ (111) surface termination. $E_{\text{slab}}^{\text{rel}}(\Psi)$ is the Al- or YO_3 -terminated $YAlO_3$ (111) slab total energy after the atomic relaxation. The $E_{\text{slab}}^{\text{unrel}}(\Psi)$ is the Al- or YO_3 -terminated $YAlO_3$ (111) slab total energy before the atomic relaxation. The factor of $\frac{1}{2}$ comes from the fact that two surfaces are created due to the crystal cleavage. Finally, when we know the cleavage and relaxation energies, the surface energy is calculated as the sum of them

$$E_{\text{surf}}(\Psi) = E_{\text{cl}}(YO_3 + \text{Al}) + E_{\text{rel}}(\Psi). \quad (3)$$

3. *Ab Initio* Calculation Results for $YAlO_3$ (111) Surfaces.

Comparison with $YAlO_3$ (001) as well as $SrTiO_3$, $BaTiO_3$ and $BaZrO_3$ (001) and (111) Surfaces

As a starting point of *ab initio* B3LYP calculations, we calculated the $YAlO_3$ bulk lattice constant (3.712 Å). We used calculated theoretical $YAlO_3$ bulk lattice constant in the following $YAlO_3$ polar (111) surface structure calculations. In order to describe the chemical bonding and covalency effects, we used the classical Mulliken bond population analysis for the atomic charges Q and bond populations P as described in Refs. 57 and 58. Calculated effective charges for the $YAlO_3$ bulk atoms are equal to (+2.523 e) for the Y atom, (+2.216 e) for the Al atom, and finally (-1.580 e) for the O atom. Calculated $YAlO_3$ bulk chemical bond population between Al and O atoms is equal to (+0.170 e), and it is considerably smaller, only (+0.010 e) between the Y and O atoms. Calculated $YAlO_3$ bulk optical band by means of the B3LYP method at Γ point is equal to 6.21 eV.

According to the results of performed calculations for Al-terminated $YAlO_3$ (111) surface (Table 1), the upper layer Al atom is strongly (by 4.85% of bulk lattice constant a_0) displaced inwards toward the bulk. The second layer metal Y atom is displaced inwards even more strongly (by 6.47% of a_0). The second layer O atom is displaced very slightly outwards (by 0.06% of a_0). The third layer Al atom, in contrast to the first layer Al atom, rather strongly (by 2.42% of a_0) is displaced outwards. As we can see from Table 1, according to performed calculations for all four materials, first and second layer metal atoms are strongly displaced inwards,

Table 1. Calculated displacement of Al-, Ti- and Zr-terminated YAlO_3 , SrTiO_3 , BaTiO_3 and BaZrO_3 (111) surface upper three layer atoms (as a percentage of the bulk crystal lattice constant $a_0 = 3.712, 3.914, 4.021, 4.234 \text{ \AA}$, respectively). Positive (negative) values describe atomic displacements in the direction outwards (inwards) of the surface.

Material		YAlO_3	SrTiO_3	BaTiO_3	BaZrO_3
Layer	Ion	Displacement (Δz)	Displacement (Δz)	Displacement (Δz)	Displacement (Δz)
1	B	-4.85	-3.58	-11.19	-8.03
2	A	-6.47	-11.24	-6.22	-9.73
	O	+0.06	+1.53	+2.74	+0.78
3	B	+2.42	+0.26	-0.25	-0.02

Table 2. Calculated displacement of YO_3 -, SrO_3 - and BaO_3 -terminated YAlO_3 , SrTiO_3 , BaTiO_3 and BaZrO_3 (111) surface upper three layer atoms (as a percentage of the bulk crystal lattice constant $a_0 = 3.712, 3.914, 4.021, 4.234 \text{ \AA}$, respectively). Positive (negative) values describe atomic displacements in the direction outwards (inwards) of the surface.

Material		YAlO_3	SrTiO_3	BaTiO_3	BaZrO_3
Layer	Ion	Displacement (Δz)	Displacement (Δz)	Displacement (Δz)	Displacement (Δz)
1	A	-1.51	+1.33	-1.24	+1.70
	O	-0.16	-0.03	-3.98	-0.57
2	B	+0.19	+1.81	+2.49	+0.21
3	A	+0.78	-0.03	+1.49	+0.71
	O	+0.11	-0.26	-0.25	-0.01

while all second layer O atoms are displaced outwards by much smaller displacement magnitude than the metal atoms inwards.

For YO_3 -terminated YAlO_3 (111) surface, both upper layer atoms are displaced inwards, whereas all second and third layer atoms are displaced outwards (Table 2). Namely, the upper layer metal atom Y is displaced inwards by 1.51% of a_0 and also the oxygen atom slightly, only by 0.16% of a_0 , is displaced inwards. All second and third layer atoms are displaced outwards, but by rather small displacement magnitudes less than 1% of a_0 (Table 2). It is worth noting that for all four calculated perovskites (Table 2), the first layer oxygen atoms are displaced inwards, while all second layer atoms are displaced outwards.

With the aim to compare the calculated and experimental SrTiO_3 (001) surface structures, the surface rumpling s (the relative displacement of the metal atom with respect to oxygen in the upper surface layer) as well as the changes in the interlayer distances Δd_{ij} (where i and j are numbers of layers) are collected in Table 3. Calculated interlayer distances are based on the positions of displaced metal atoms, which as we know are much better electron scatterers than oxygen atoms.⁵⁹ As we can see from Table 3, the agreement is fairly good for all theoretical calculation methods, which give the same sign for the surface rumpling as well as the changes of the interlayer distances. For example, the surface rumpling s for the SrO-terminated surface is calculated to be much larger than for the TiO_2 -terminated SrTiO_3 (001) surface by all theoretical methods.⁶⁰⁻⁶³ As we can see from Table 3, both calculated

Table 3. Calculated and experimental surface rumpling s and relative displacements Δd_{ij} (in percent of the bulk lattice constant) for the upper three surface planes of SrO- and TiO_2 -terminated SrTiO_3 (001) slabs.

SrTiO_3	SrO-terminated SrTiO_3 (001)			TiO_2 -terminated SrTiO_3 (001)		
	s	Δd_{12}	Δd_{23}	s	Δd_{12}	Δd_{23}
This work	5.66	-6.58	1.75	2.12	-5.79	3.55
Shell model ⁶⁰	8.2	-8.6	3.0	1.2	-6.4	4.0
HF-LYP ⁶¹	3.8	-4.3	1.3	1.2	-4.9	2.2
<i>Ab initio</i> ⁶²	5.8	-6.9	2.4	1.8	-5.9	3.2
<i>Ab initio</i> ⁶³	7.7	-8.6	3.3	1.5	-6.4	4.9
LEED exp ⁵⁹	4.1 ± 2	-5 ± 1	2 ± 1	2.1 ± 2	1 ± 1	-1 ± 1
RHEED exp ⁶⁴	4.1	2.6	1.3	2.6	1.8	1.3
MEIS exp ⁶⁵				1.5 ± 0.2	0.5 ± 0.2	
SXRD exp ⁶⁶	1.3 ± 12.1	-0.3 ± 3.6	-6.7 ± 2.8	12.8 ± 8.5	0.3 ± 1	

TiO_2 - and SrO-terminated (001) SrTiO_3 surfaces exhibit a reduction of interlayer distance Δd_{12} and an expansion of Δd_{23} .

The calculated surface rumpling amplitudes s for both SrTiO_3 (001) surface terminations are in fair agreement with the LEED, RHEED, MEIS and SXRD experiments^{59,64-66} (Table 3). Nevertheless, the calculated changes in interlayer distances are in disagreement with the LEED experiments⁵⁹ for the TiO_2 -terminated SrTiO_3 (001) surface, which show an expansion of the Δd_{12} and a reduction of Δd_{23} . In contrast, all *ab initio* as well as classical shell model calculations show a reduction of interlayer distance Δd_{12} and an expansion of Δd_{23} (Table 3). Nevertheless, as we can see from Table 3, unfortunately, the different experiments contradict each other with respect the sign of Δd_{12} and Δd_{23} for the SrO-terminated SrTiO_3 (001) surface, and for sign of Δd_{23} of the TiO_2 -terminated SrTiO_3 (001) surface.

Calculated surface relaxation energy for Al-terminated YAlO_3 (111) surface (-1.24 eV) is more than seventeen times larger than the surface relaxation energy for YO_3 -terminated YAlO_3 (111) surface (-0.07 eV) (Table 4). Calculated surface energy for the YO_3 -terminated YAlO_3 (111) surface is equal to 9.26 eV/cell and thereby it by 1.17 eV/cell exceeds the surface energy for Al-terminated YAlO_3 (111) surface 8.09 eV/cell (Table 4).

Calculated YO_3 - and Al-terminated YAlO_3 (111) surface energies (9.26 and 8.09 eV/cell) (Table 4) are considerably larger than the YO- and AlO_2 -terminated YAlO_3 (001) surface energies (2.33 and 3.31 eV/cell) (Table 5 and Fig. 3). Also for another calculated SrTiO_3 , BaTiO_3 and BaZrO_3 perovskites, their (111) surface energies for both AO_3 and B-terminations (Table 4) are always larger than their relevant surface energies for both AO- and BO_2 -terminated (001) surfaces (Table 5). From Table 4 we can see that the AO_3 -terminated perovskite (111) surface energies are always larger than the B-terminated surface energies for YAlO_3 , SrTiO_3 , BaTiO_3 and BaZrO_3 perovskites (Table 4). It is worth noting that the ABO_3 perovskite (001) surface energies are also always smaller than the ABO_3 perovskite (011) surface energies.¹⁶ The only exception is calculations by Zhang *et al.*,⁶⁷ where

Table 4. Calculated cleavage, relaxation, and surface energies for YAlO_3 , SrTiO_3 , BaTiO_3 as well as BaZrO_3 (111) surfaces (in electron volt per surface cell).

Surface (111)	E_{cl} (AO_3+B)	Termination	E_{rel}	E_{surf} (111)
YAlO_3	9.33	Al-terminated	-1.24	8.09
		YO_3 -terminated	-0.07	9.26
SrTiO_3	6.65	Ti-terminated	-1.66	4.99
		SrO_3 -terminated	-0.35	6.30
BaTiO_3	9.22	Ti-terminated	-1.94	7.28
		BaO_3 -terminated	-0.82	8.40
BaZrO_3	9.43	Zr-terminated	-1.49	7.94
		BaO_3 -terminated	-0.10	9.33

Table 5. Calculated surface energies for YAlO_3 , SrTiO_3 , BaTiO_3 as well as BaZrO_3 (001) surfaces (in electron volt per surface cell).

Surface (001)	Termination	E_{surf} (001)
YAlO_3	YO-terminated	2.33
	AlO_2 -terminated	3.31
SrTiO_3	SrO-terminated	1.15
	TiO_2 -terminated	1.23
BaTiO_3	BaO-terminated	1.19
	TiO_2 -terminated	1.07
BaZrO_3	BaO-terminated	1.30
	ZrO_2 -terminated	1.31

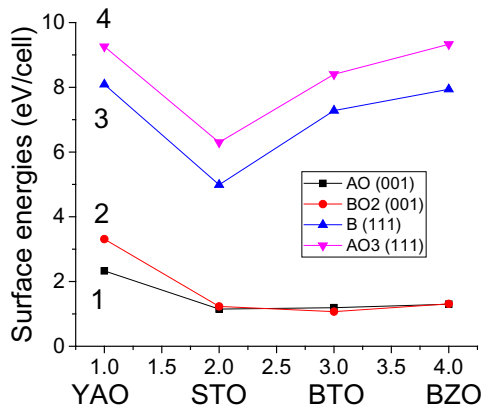
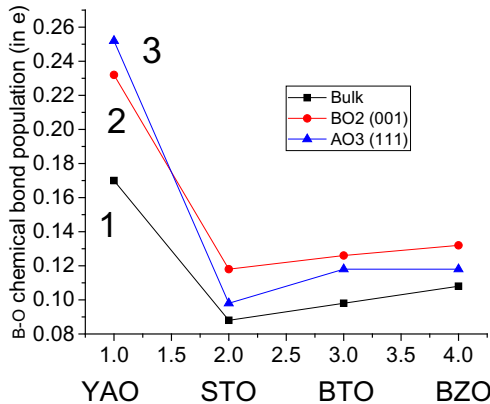


Fig. 3. (Color online) Our calculated surface energies (in eV/cell) for AO- (1) and BO_2 -terminated (2) (001) as well as B- (3) and AO_3 -terminated (4) (111) surfaces of YAlO_3 , SrTiO_3 , BaTiO_3 and BaZrO_3 perovskites by means of the hybrid B3LYP or B3PW exchange-correlation functionals.

Table 6. Calculated B–O chemical bond population of YAlO_3 , SrTiO_3 , BaTiO_3 and BaZrO_3 perovskite bulk, BO_2 -terminated (001) as well as AO_3 -terminated (111) surfaces (in e).

B–O bond population	YAlO_3	SrTiO_3	BaTiO_3	BaZrO_3
Bulk	+0.170	+0.088	+0.098	0.108
BO_2 -terminated (001)	+0.232	+0.118	+0.126	0.132
AO_3 -terminated (111)	+0.252	+0.098	+0.118	0.118


 Fig. 4. (Color online) Calculated bulk (1) as well as BO_2 -terminated (001) (2) and AO_3 -terminated (111) surface B–O chemical bond populations (in e) for YAlO_3 , SrTiO_3 , BaTiO_3 and BaZrO_3 perovskites.

they found that the A-type O-terminated CaTiO_3 (011) surface energy is smaller than the TiO_2 -terminated CaTiO_3 (001) surface energy.

The covalent nature of the chemical bonding between Al and O atoms in the YAlO_3 bulk is confirmed by the large bond population values between Al and O atoms (+0.170 e) (Table 6 and Fig. 4). This Al–O bond population valued for the YAlO_3 bulk is considerably larger than the relevant B–O chemical bond population for another our calculated SrTiO_3 , BaTiO_3 and BaZrO_3 perovskites (0.088, 0.098 and 0.108 e , respectively). The Al–O chemical bond population near the AlO_2 -terminated YAlO_3 (001) surface is 1.36 times larger than in the YAlO_3 bulk (Table 6). Nevertheless, the Al–O chemical bond population reach its maximal value near the YO_3 -terminated YAlO_3 (111) surface and is equal to (0.252 e), or in another words, it is 1.48 times larger than in the YAlO_3 bulk. It is interesting to notice, that also for another our calculated SrTiO_3 , BaTiO_3 and BaZrO_3 perovskites the B–O chemical bond population near the (001) and (111) surfaces is considerably larger than in the bulk. Nevertheless, for SrTiO_3 , BaTiO_3 and BaZrO_3 perovskites, in contrast to YAlO_3 , the B–O chemical bond population near the (001) surfaces is larger than near the (111) surfaces.

By means of the B3LYP functional calculated SrTiO_3 bulk bandgap (3.99 eV) is only by 0.24 eV or approximately 6.4% overestimated regarding the experimental

Table 7. Calculated optical bandgaps at the Γ -point for YAlO_3 , SrTiO_3 , BaTiO_3 and BaZrO_3 bulk as well as AO_3 - and B-terminated (111) and BO_2 - and AO-terminated (001) surfaces (in eV).

Optical bandgap	YAlO_3	SrTiO_3	BaTiO_3	BaZrO_3
Bulk	6.21	3.99	3.55	4.79
AO_3 -terminated (111)	4.57	3.72	3.60	4.51
B-terminated (111)	5.95	3.98	4.14	4.47
AO-terminated (001)	6.02	3.72	3.49	4.71
BO_2 -terminated (001)	6.41	3.95	2.96	4.37
Experiment	8.5 ^a	3.75 ^b	2.84 ^c	5.3 ^d

Notes: ^aRef. 71, ^bRef. 68, ^cRef. 70, ^dRef. 69.

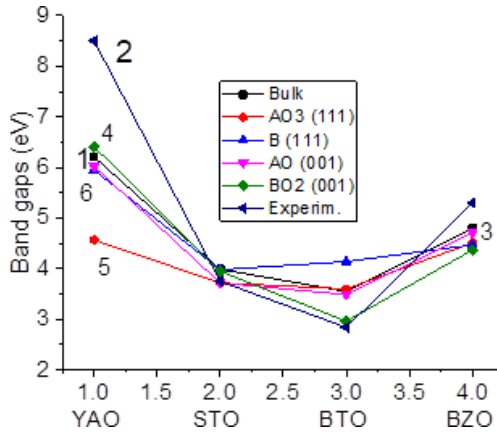


Fig. 5. (Color online) Calculated (1) and experimental (2) bulk as well as calculated AO (3) and BO_2 -terminated (4) (001), AO_3 (5) and B-terminated (6) (111) surface Γ - Γ bandgaps (in eV) for YAlO_3 , SrTiO_3 , BaTiO_3 and BaZrO_3 perovskites.

bulk bandgap value of 3.75 eV⁶⁸ (Table 7 and Fig. 5). Also for BaZrO_3 bulk, by means of the B3LYP method calculated bandgap (4.79 eV) is only by 0.51 eV or 9.6% underestimated regarding the experimental bulk bandgap value of 5.3 eV⁶⁹ (Table 7). According to the recent experimental data, the BaTiO_3 bulk bandgap in its cubic phase is equal to approximately 2.84 eV.⁷⁰ We compared the B3LYP calculation result for YAlO_3 bulk bandgap in the cubic phase with the experimental result obtained for its orthorhombic phase 8.5 eV.⁷¹

Calculated ABO_3 optical bandgaps near the (001) surfaces as a rule are smaller than the ABO_3 perovskite bulk bandgaps. The single exception is the YAlO_3 perovskite AlO_2 -terminated (001) surface bandgap (6.41 eV), which by 0.2 eV exceeds the YAlO_3 bulk bandgap value (6.21 eV). Also for YAlO_3 , SrTiO_3 and BaZrO_3 perovskite (111) surfaces, our calculated bandgap near the (111) surfaces is reduced with respect to the bulk bandgap value. The only exception from this tendency is increase of our calculated bandgaps near the BaTiO_3 (111) surfaces.

4. Summary and Conclusions

We performed a large amount of B3LYP and B3PW calculations for YAlO_3 , SrTiO_3 , BaTiO_3 and BaZrO_3 (001) and (111) surfaces, and as a result detected following systematic trends:

- (1) The relaxation of (001) and (111) surface metal atoms for YAlO_3 , SrTiO_3 , BaTiO_3 and BaZrO_3 perovskite, in the upper three surface layers for both AO and BO_2 (001) as well as AO_3 and B (111) surface terminations, in most cases, are considerably larger than that of oxygen atoms.
- (2) For the AO- and BO_2 -terminated (001) as well as AO_3 - and B-terminated (111) surfaces of YAlO_3 , SrTiO_3 , BaTiO_3 and BaZrO_3 perovskites, the systematic trend, with a few exceptions, according to performed B3LYP and B3PW calculations, is that all atoms of the upper surface layer relax inward, whereas all atoms of the second surface layer relax outward.
- (3) The YAlO_3 , SrTiO_3 , BaTiO_3 and BaZrO_3 (001) surface energies for both calculated AO and BO_2 -terminations, in most cases, are almost equal. In contrast, the (111) surface energies for both AO_3 and B-terminations are quite different, also the AO_3 -terminated (111) surface energies are always considerably larger than the B-terminated (111) surface energies. Calculated AO_3 - and B-terminated (111) surface energies always are much larger than the AO- and BO_2 -terminated (001) surface energies.
- (4) The B–O chemical bond population in YAlO_3 , SrTiO_3 , BaTiO_3 and BaZrO_3 perovskite bulk are always smaller than near the (111) and especially the (001) surfaces. In most cases the B–O chemical bond population near the (001) surfaces are slightly larger than near the (111) surfaces.
- (5) As follows from the performed B3LYP and B3PW calculations for YAlO_3 , SrTiO_3 , BaTiO_3 and BaZrO_3 perovskites, the AO- and BO_2 -terminated (001) as well as AO_3 - and B-terminated (111) surface bandgaps are always reduced with respect to their bulk bandgap values. The only exceptions are the BaTiO_3 (111) surface bandgaps as well as BO_2 -terminated YAlO_3 (001) surface bandgaps.

Acknowledgments

We greatly acknowledge the financial support via Latvian-Ukrainian Joint Research Project No. LV-UA/2018/2, Latvian Council of Science Grant No. 2018/2-0083 “Theoretical prediction of hybrid nanostructured photocatalytic materials for efficient water splitting”, Latvian Council of Science Grant No. 2018/1-0214 as well as ERAF Project No. 1.1.1.1/18/A/073.

References

1. M. Dawber, K. M. Rabe and J. F. Scott, *Rev. Mod. Phys.* **77**, 1083 (2005).
2. S. E. Reyes-Lillo, K. M. Rabe and J. B. Neaton, *Phys. Rev. Mater.* **3**, 030601 (2019).

3. Y. A. Mastrikov et al., *J. Mater. Chem. A* **6**, 11929 (2018).
4. C. G. Ma, V. Krasnenko and M. G. Brik, *J. Phys. Chem. Solids* **115**, 289 (2018).
5. R. I. Eglitis and D. Vanderbilt, *Phys. Rev. B* **76**, 155439 (2007).
6. W. Jia et al., *J. Lumin.* **83–84**, 109 (1999).
7. J. Meng et al., *J. Mater. Sci.* **54**, 1967 (2019).
8. R. I. Eglitis, *Int. J. Mod. Phys. B* **28**, 1430009 (2014).
9. R. A. P. Ribeiro et al., *Appl. Surf. Sci.* **452**, 463 (2018).
10. B. C. Luo et al., *Appl. Surf. Sci.* **351**, 558 (2015).
11. R. Eglitis, *Int. J. Mod. Phys. B* **33**, 1950151 (2019).
12. Z. Zhao et al., *Phys. Rev. Mater.* **3**, 043601 (2019).
13. M. Sokolov et al., *Int. J. Mod. Phys. B* **31**, 1750251 (2017).
14. E. A. Kotomin et al., *Phys. Chem. Chem. Phys.* **10**, 4258 (2008).
15. M. V. Ananev et al., *Russ. J. Electrochem.* **48**, 879 (2012).
16. R. I. Eglitis et al., *J. Mater. Sci.* **55**, 203 (2020).
17. N. M. Porotnikova, M. V. Ananev and E. Kh. Kurumchin, *Russ. J. Electrochem.* **47**, 1250 (2011).
18. R. I. Eglitis and A. I. Popov, *J. Nano-Electron. Phys.* **11**, 01001 (2019).
19. H. Y. Hwang et al., *Nat. Mater.* **11**, 103 (2012).
20. T. Matsuda et al., *J. Alloys Compd.* **351**, 43 (2003).
21. Z. Zhang et al., *Adv. Energy Mater.* **7**, 1700242 (2017).
22. A. A. Emery and C. Wolverton, *Sci. Data* **4**, 170153 (2017).
23. K. Szot et al., *Appl. Phys. A* **62**, 335 (1996).
24. J. Druce et al., *Energy Environ. Sci.* **7**, 3593 (2014).
25. G. Z. Zhu, G. Radtke and G. A. Botton, *Nature* **490**, 384 (2012).
26. M. S. J. Marshall et al., *Phys. Rev. B* **83**, 035410 (2011).
27. Y. Y. Lin et al., *Surf. Sci.* **605**, L51 (2011).
28. R. Shimizu et al., *Appl. Phys. Lett.* **100**, 263106 (2012).
29. R. I. Eglitis and D. Vanderbilt, *Phys. Rev. B* **77**, 195408 (2008).
30. R. I. Eglitis and D. Vanderbilt, *Phys. Rev. B* **78**, 155420 (2008).
31. M. G. Brik, C. G. Ma and V. Krasnenko, *Surf. Sci.* **608**, 146 (2013).
32. E. A. Kotomin et al., *Thin Solid Films* **400**, 76 (2001).
33. K. Yang et al., *Int. J. Mod. Phys. B* **30**, 1650168 (2016).
34. R. I. Eglitis, *J. Phys.: Condens. Matter* **19**, 356004 (2007).
35. M. Saghayezhian et al., *J. Phys. Chem. C* **123**, 8086 (2019).
36. R. I. Eglitis and A. I. Popov, *J. Saudi Chem. Soc.* **22**, 459 (2018).
37. J. R. Sambrano et al., *J. Mol. Struct.* **813**, 49 (2007).
38. G. Borstel et al., *Phys. Stat. Sol. B* **236**, 253 (2003).
39. R. I. Eglitis and A. I. Popov, *Nucl. Instr. Meth. B* **434**, 1 (2018).
40. N. Sivadas et al., *Phys. Rev. B* **89**, 075303 (2014).
41. R. I. Eglitis, *Appl. Surf. Sci.* **358**, 556 (2015).
42. W. Liu et al., *Solid State Commun.* **149**, 1871 (2009).
43. R. I. Eglitis, *Solid State Ion.* **230**, 43 (2013).
44. J. Feng, X. Zhu and J. Guo, *Surf. Sci.* **614**, 38 (2013).
45. R. I. Eglitis, *Phys. Stat. Sol. B* **252**, 635 (2015).
46. Y. Liang et al., *Sci. Rep.* **5**, 10634 (2015).
47. R. I. Eglitis, *Ferroelectrics* **483**, 53 (2015).
48. G. M. Vanacore, L. F. Zagonel and N. Barrett, *Surf. Sci.* **604**, 1674 (2010).
49. A. Pojani, F. Finocchi and C. Noguera, *Surf. Sci.* **442**, 179 (1999).
50. A. Pojani, F. Finocchi and C. Noguera, *Appl. Surf. Sci.* **142**, 177 (1999).
51. V. R. Saunders et al., *CRYSTAL User Manual* (University of Torino, Italy, 2009).

52. A. D. Becke, *J. Chem. Phys.* **98**, 5648 (1993).
53. C. Lee, W. Yang and R. G. Parr, *Phys. Rev. B* **37**, 785 (1988).
54. H. J. Monkhorst and J. D. Pack, *Phys. Rev. B* **13**, 5188 (1976).
55. R. I. Eglitis *et al.*, *Ceram. Int.* **30**, 1989 (2004).
56. S. Piskunov *et al.*, *Surf. Sci.* **575**, 75 (2005).
57. C. R. A. Catlow and A. M. Stoneham, *J. Phys. C: Solid State Phys.* **16**, 4321 (1983).
58. R. C. Bochiccio and H. F. Reale, *J. Phys. B: At. Mol. Opt. Phys.* **26**, 4871 (1993).
59. N. Bickel *et al.*, *Phys. Rev. Lett.* **62**, 2009 (1989).
60. E. Heifets, E. A. Kotomin and J. Maier, *Surf. Sci.* **462**, 19 (2000).
61. E. Heifets *et al.*, *Phys. Rev. B* **64**, 235417 (2001).
62. J. Padilla and D. Vanderbilt, *Surf. Sci.* **418**, 64 (1998).
63. C. Cheng, K. Kunc and M. H. Lee, *Phys. Rev. B* **62**, 10409 (2000).
64. T. Hikita *et al.*, *Surf. Sci.* **287–288**, 377 (1993).
65. A. Ikeda *et al.*, *Surf. Sci.* **433**, 520 (1999).
66. G. Charlton *et al.*, *Surf. Sci.* **457**, L376 (2000).
67. M. Zhang *et al.*, *Phys. Rev. B* **76**, 115426 (2007).
68. K. van Benthem, C. Elsässer and R. H. French, *J. Appl. Phys.* **90**, 6156 (2001).
69. J. Robertson, *J. Vacuum Sci. Technol. B* **18**, 1785 (2000).
70. V. Mishra *et al.*, *J. Appl. Phys.* **122**, 065105 (2017).
71. C. Lushchik *et al.*, *J. Phys.: Condens. Matter* **6**, 11187 (1994).